

Fast Sparse Matrix Permutation for Mesh-Based Direct Solvers

BEHROOZ ZAREBAVANI*, University of Toronto, Canada

AHMED H. MAHMOUD*, Massachusetts Institute of Technology, USA

ANA DODIK, Massachusetts Institute of Technology, USA

CHANGCHENG YUAN, Texas A&M University, USA

SERBAN D. PORUMBESCU, University of California, Davis, USA

JOHN D. OWENS, University of California, Davis, USA

MARYAM MEHRI DEHNAVI†, University of Toronto, Canada and NVIDIA Research, USA

JUSTIN SOLOMON†, Massachusetts Institute of Technology, USA

We present a fast sparse matrix permutation algorithm tailored to linear systems arising from triangle meshes. Our approach produces nested-dissection-style permutations while significantly reducing permutation runtime overhead. Rather than enforcing strict balance and separator optimality, the algorithm deliberately relaxes these design decisions to favor fast partitioning and efficient elimination-tree construction. Our method decomposes permutation into patch-level local orderings and a compact quotient-graph ordering of separators, preserving the essential structure required by sparse Cholesky factorization while avoiding its most expensive components. We integrate our algorithm into vendor-maintained sparse Cholesky solvers on both CPUs and GPUs. Across a range of graphics applications, including single factorizations and repeated factorizations, our method reduces permutation time and improves the sparse Cholesky solve performance by up to 6.27 \times . Our code is available at <https://github.com/BehroozZare/fast-permute>.

CCS Concepts: • **Mathematics of computing** \rightarrow *Solvers*; • **Computing methodologies** \rightarrow *Linear algebra algorithms*; **Parallel algorithms**.

ACM Reference Format:

Behrooz Zarebavani, Ahmed H. Mahmoud, Ana Dodik, Changcheng Yuan, Serban D. Porumbescu, John D. Owens, Maryam Mehri Dehnavi, and Justin Solomon. 2026. Fast Sparse Matrix Permutation for Mesh-Based Direct Solvers. In *Special Interest Group on Computer Graphics and Interactive Techniques Conference Conference Papers (SIGGRAPH Conference Papers '26)*, July 19–23, 2026, Los Angeles, CA, USA. ACM, New York, NY, USA, 16 pages. <https://doi.org/10.1145/3799902.3811189>

*Joint first author

†Joint last author

Authors' Contact Information: Behrooz Zarebavani, Department of Computer Science, University of Toronto, Toronto, ON, Canada, behrooz.zarebavani@gmail.com; Ahmed H. Mahmoud, Computer Science & Artificial Intelligence Laboratory, Massachusetts Institute of Technology, Cambridge, MA, USA, ahdhn@mit.edu; Ana Dodik, Computer Science & Artificial Intelligence Laboratory, Massachusetts Institute of Technology, Cambridge, MA, USA, anadodik@mit.edu; Changcheng Yuan, Department of Computer Science and Engineering, Texas A&M University, College Station, TX, USA, eric.yuan.cc@gmail.com; Serban D. Porumbescu, Department of Electrical and Computer Engineering, University of California, Davis, CA, USA, sdporumbescu@ucdavis.edu; John D. Owens, Department of Electrical and Computer Engineering, University of California, Davis, CA, USA, jowens@ece.ucdavis.edu; Maryam Mehri Dehnavi, Department of Computer Science, University of Toronto, Toronto, ON, Canada, mmehride@cs.toronto.edu and NVIDIA Research, USA, mdehnavi@nvidia.com; Justin Solomon, Computer Science & Artificial Intelligence Laboratory, Massachusetts Institute of Technology, Cambridge, MA, USA, jsolomon@mit.edu.



This work is licensed under a Creative Commons Attribution 4.0 International License.

SIGGRAPH Conference Papers '26, Los Angeles, CA, USA

© 2026 Copyright held by the owner/author(s).

ACM ISBN 979-8-4007-2554-8/2026/07

<https://doi.org/10.1145/3799902.3811189>

1 Introduction

Sparse linear solvers are central computational kernels in computer graphics. Many mesh-centric workloads (e.g., parameterization, deformation, physical simulation, and geometric flows) solve large positive semidefinite systems, for which sparse Cholesky factorization is often the most practical and convenient choice due to its robustness. Nevertheless, in many graphics pipelines, overall runtime remains dominated by the cost of the linear solver.

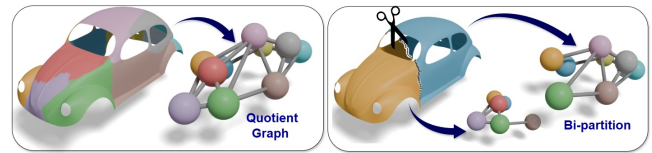
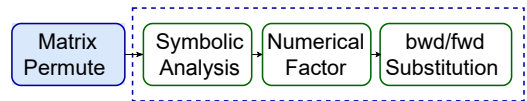


Fig. 1. Scalable fill-reducing permutation computation on a triangular mesh. Our patch-based, nested-dissection-style method compresses the triangular mesh domain into a small quotient graph and reuses this compression across recursive calls, improving scalability over state-of-the-art methods. We achieve a 6.62 \times speedup over the highly optimized NVIDIA cuDSS by accelerating its permutation computation.



Sparse Cholesky factorization pipeline.

Sparse Cholesky solvers are often accelerated by amortizing an upfront symbolic analysis phase that inspects the sparsity pattern and prepares data structures for efficient factorization and forward/backward solves. While recent solvers like Apple Accelerate [Apple Inc. 2025], Intel MKL [Intel Corporation 2025], and NVIDIA cuDSS [NVIDIA Corporation 2025] significantly improve the symbolic and numerical stages, the symbolic phase still contains a key scalability bottleneck, i.e., computing a *fill-reducing permutation*. Permutation is an essential preprocessing step in the symbolic phase; it reorders the rows and columns of the matrix to make the Cholesky factors as sparse as possible. In our experiments (see Figure 2), permutation accounts for an average of 86% of the total runtime, reaching 96% for large meshes in the newly-introduced, highly-optimized NVIDIA cuDSS solver.

Finding the optimal fill-reducing permutation is NP-complete [Yan-nakakis 1981], so practical solvers rely on heuristics [Davis 2006]. High-performance solvers predominantly use nested dissection (e.g.,

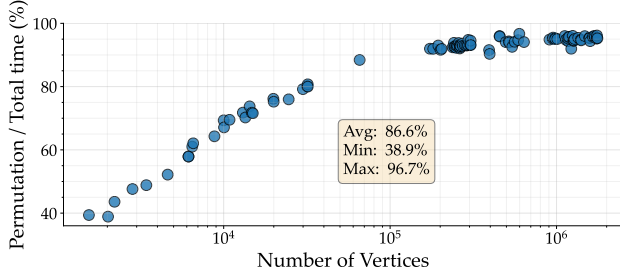


Fig. 2. Fraction of time spent on matrix permutation to end-to-end time for solving mean curvature flow [Desbrun et al. 1999] for different inputs.

METIS [Karypis et al. 2013a]) or minimum-degree orderings (e.g., AMD [Amestoy et al. 1996]). Nested dissection typically yields higher-quality orderings and enables parallel factorization via its hierarchical structure, while AMD has low ordering cost but can produce higher fill-in on mesh-like problems [Lipton et al. 1979].

In current practice, permutation is treated as a standalone preprocessing step and applied as a black box before symbolic analysis. This separation leads to loss of nested-dissection hierarchical information, which can be reused in permutation and symbolic analysis. For example, NVIDIA cuDSS requires this structure in the form of an *elimination tree* for its symbolic analysis. This separation creates a gap between high-quality orderings that also provide reusable hierarchy information for symbolic analysis, and faster orderings that focus on permutation alone. The latter not only tend to increase fill-in, but also force solvers to recompute symbolic structures that could otherwise be reused from a nested-dissection hierarchy.

In this paper, we introduce a sparse matrix permutation algorithm tailored to mesh-derived linear systems. Our method produces nested-dissection-style orderings that exploit mesh structure while remaining efficient to compute. Crucially, it preserves the reusable separator hierarchy needed for symbolic analysis, while achieving a better quality–runtime trade-off through faster separator computation and efficient integration of minimum-degree techniques such as AMD. Compared to state-of-the-art permutation tools, our algorithm achieves up to 10.27× speedup (4.58× geometric mean) in ordering time and delivers up to 6.62× end-to-end speedup (3.51× geometric mean) when solving linear systems.

Our key insight is that nested-dissection permutation is often dominated by the effort spent enforcing strict balance and minimizing separator size, as done by general-purpose partitioners such as METIS [Karypis et al. 2013a] and PT-Scotch [Chevalier and Pellegrini 2008]. For mesh-derived systems, relaxing these constraints dramatically reduces permutation time; although this produces lower-quality separators, the reduced preprocessing overhead outweighs the increased fill-in in practice. This motivates a multi-stage permutation strategy that decouples ordering speed from ordering quality while retaining reusable symbolic structure. In particular, our method constructs the *elimination tree* alongside the permutation, enabling direct reuse for symbolic scheduling and jointly accelerating both permutation and symbolic analysis. Our code is available at <https://github.com/BehroozZare/fast-permute>.

2 Background

Given a sparse symmetric matrix $A \in \mathbb{R}^{n \times n}$, we define an undirected graph $G = (V_G, E_G)$ where each vertex $i \in V_G$ corresponds to row/column i of A , and there is an edge $(i, j) \in E_G$ if and only if $A_{ij} \neq 0$. We refer to G as the *graph* of A .

Nested dissection [Lipton et al. 1979] recursively partitions G by finding a small set of vertices S (i.e., *separators*) whose removal separates G into two subgraphs, g_1 and g_2 (see Figure 4). The resulting permutation orders the vertices in g_1 and g_2 before the vertices in S . During Cholesky factorization, this means that the unknowns associated with g_1 and g_2 are eliminated first and the separator unknowns are eliminated later [Scott and Tuma 2023]. The dependencies induced by this elimination order are captured by the *elimination tree* (etree): its nodes represent elimination groups (i.e., blocks of rows/columns) and its edges indicate that eliminating one group produces updates to another. For a single dissection, g_1 and g_2 form two independent subproblems that meet at the separator S (the parent). Thus, fill-in is created only within g_1 , within g_2 , and within the separator block, there is no fill-in between g_1 and g_2 (see Figure 3). Nested dissection repeats this process recursively on the subgraphs until reaching a prescribed stopping criterion (e.g., recursion depth).

Many sparse linear systems in geometry processing arise from FEM discretizations. For such operators (e.g., Laplace–Beltrami), there is a one-to-one correspondence between mesh vertices and unknowns (rows/columns) in the sparse linear system, and thus between mesh vertices and the vertices of G . In this setting, G matches the mesh adjacency graph. We exploit this correspondence to move between the mesh and the matrix graph.

Finally, we define a *patch* as a connected subset of mesh vertices V_M . Formally, a patch $P \subseteq V_M$ is a set of vertices whose induced submesh is connected. A collection of patches $\{P_k\}$ forms a partition of the mesh if $\bigcup_k P_k = V_M$ and $P_k \cap P_\ell = \emptyset$ for $k \neq \ell$. Each patch induces a subgraph of G through $V_M \leftrightarrow V_G$ mapping. The *quotient graph* is the graph whose nodes correspond to patches and whose edges capture patch adjacency induced by edges in G .

3 Related Work

Finding a permutation that minimizes fill-in is NP-complete [Ashkiani et al. 2018]. Exact methods based on nonserial dynamic programming [Bertelè and Brioschi 1969, 1972] do not scale and are not used in practice. Practical solvers rely on heuristics. Bichot and Siarry [2013] and Schulz and Strash [2018] give an overview of fill-reducing orderings. We review widely-used matrix permutation techniques followed by prior work that leverages nested dissection in symbolic analysis.

Minimum-degree orderings. Minimum-degree (MD) methods construct an elimination order by repeatedly selecting a vertex with (approximately) minimum degree in the graph, aiming to introduce the fewest fill edges [Tinney and Walker 1967]. Each elimination turns the vertex’s neighborhood into a clique, so degrees must be updated after every step; these updates dominate runtime and motivate fast, inexact update heuristics [Amestoy et al. 1996; George 1973; George and Liu 1980]. Approximate Minimum Degree (AMD) [Amestoy et al. 1996] is the standard implementation in practice and recent work reduces its cost via improved update strategies [Cummings

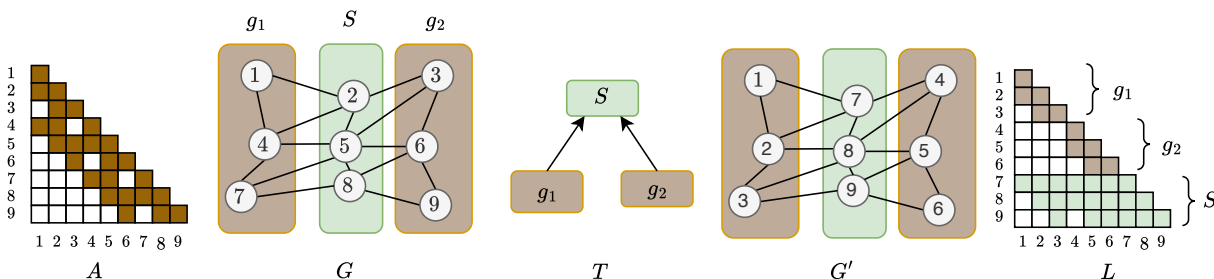


Fig. 3. **Illustration of a single nested-dissection step.** From left to right: the input matrix A , its graph G , the corresponding elimination tree T , the permuted graph G' , and the sparsity pattern of the Cholesky factor L . The separator vertices S are ordered after the vertices in g_1 and g_2 . The elimination tree encodes the dependencies induced by this order, i.e., computations for g_1 and g_2 are independent, while computations for S can proceed only after both have completed.

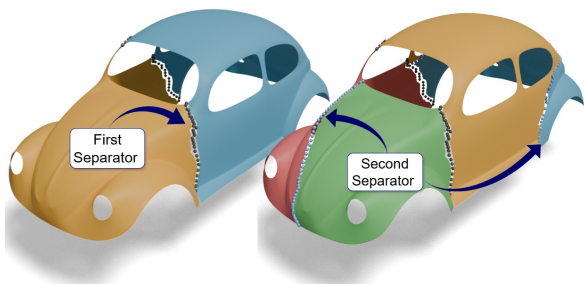


Fig. 4. **Separator set on a mesh.** Nested dissection recursively partitions the mesh by choosing small sets of vertices (shown as green points) whose removal separates the remaining mesh into disconnected subdomains. The first separator splits the mesh into two large regions (left). The second separator further partitions one of these regions (right).

et al. 2021] and GPU implementations [Chang et al. 2025]. MD methods are fast, but their local, greedy decisions can yield less balanced elimination trees and expose less parallelism than nested-dissection.

Nested dissection. Nested dissection (ND) reduces fill by recursively partitioning the matrix graph using small vertex separators and ordering separator vertices after interior vertices [George 1973]. This divide-and-conquer structure typically achieves strong fill reduction on PDE/mesh graphs and yields more parallelism due to balanced recursion [Lipton et al. 1979]. For completeness, we include a brief didactic background on how permutation affects fill-in and solver parallelism with examples in Supplemental Materials A. Modern ND implementations rely on multilevel graph partitioners that coarsen, partition, and refine the graph to compute separators efficiently. Once subgraphs become small, they often switch to simple local orderings (e.g., breadth-first variants [Cuthill and McKee 1969]). Widely used tools include METIS [Karypis et al. 2013a; Karypis and Kumar 1998], ParMETIS [Karypis et al. 2013b], and PT-Scotch [Chevalier and Pellegrini 2008].

We build on ND’s recursive structure, but observe that top levels of the recursion can dominate ordering time. Since separator computation is NP-complete, reducing the problem size can substantially accelerate this step. Accordingly, we compress the mesh into patches, reuse this patching across recursive calls, and introduce a relaxed variant improving the quality–runtime trade-off in practice.

Exploiting the ND hierarchy in symbolic analysis. Beyond producing a permutation, ND induces a hierarchy that can be reused in symbolic analysis and downstream factorization. Herholz and Alexa [2018] and Herholz and Sorkine-Hornung [2020] accelerate updates by identifying affected regions in the elimination tree and restricting refactorization and triangular solves to those regions. NASOQ [Cheshmi et al. 2020] leverages a related tree structure in constraint-based quadratic programming. Parth [Zarebavani et al. 2025] reuses the elimination tree to accelerate reordering when the sparsity pattern changes over time. Collectively, these works highlight that explicitly creating and exposing the ND-induced hierarchy enables substantial reuse beyond a one-shot ordering.

4 Our Algorithm

Overview. Our algorithm accelerates fill-reducing nested-dissection permutation by restricting separator computation to a coarse search space, i.e., the quotient graph. In the limiting case where each patch represents a single mesh vertex, our algorithm reduces to classical nested-dissection [George 1973]. However, since patches contain multiple vertices, separator decisions are made at the patch level, trading some ordering quality for a substantial reduction in permutation cost, since the size of quotient graph is significantly smaller than the input graph G . Concretely, we (i) compute a patch partition of the mesh on the GPU, (ii) lift this partition to the matrix graph to form a *group map* ($gmap$) that clusters graph vertices by patch, (iii) build an elimination tree (*etree*) using nested dissection guided by these groups, and (iv) assemble a global permutation by traversing the tree in nested-dissection order (see Algorithm 1). We use the GPU only for the first step (computing patches). The rest of the algorithm runs on the CPU.

Our design has multiple advantages. First, patches reduce the separator search space by allowing nested dissection to operate on the quotient graph rather than the full matrix graph. Since patch construction is inexpensive and highly parallel for meshes, as shown in prior work (e.g., RXMesh [Mahmoud et al. 2021], MeshTaichi [Yu et al. 2022]), this reduction dramatically decreases permutation runtime. Second, unlike classical nested-dissection implementations (e.g., METIS), which repeatedly coarsen the graph at each recursion level, our method constructs a single quotient graph and reuses it throughout the recursion. This reuse avoids redundant coarsening work and further accelerates permutation. Finally, our algorithm

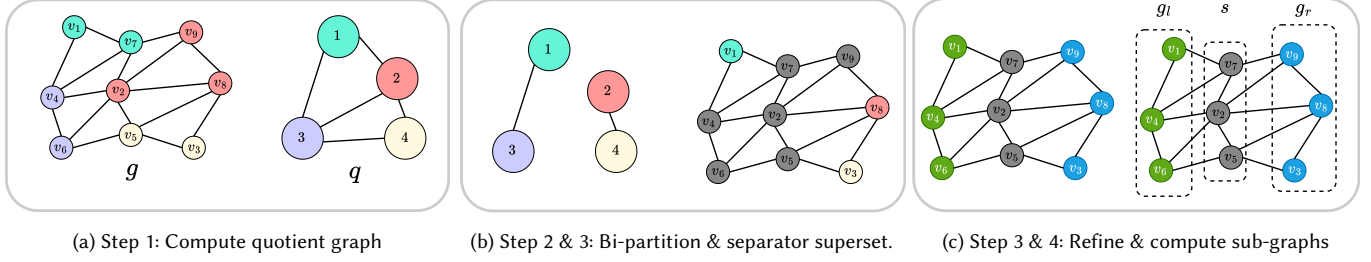


Fig. 5. **Separator computation.** For the current subgraph g , we form a quotient graph q , bipartition q , lift the partition back to V_g to obtain a separator superset, refine it to reduce its size while maintaining balance, and then extract the left and right sub-graphs for the next recursion level.

Algorithm 1 Algorithm overview.

Input: A, M, nd_level

Output: $perm, etree$

- ```

/* Step 1: Obtain a patch partition */
1: $patches \leftarrow \text{GETPATCHES}(M)$ ▷ or user-provided
/* Step 2: Build the graph and lift patches to graph groups */
2: $G, gmap \leftarrow \text{BUILDGRAPHANDGROUPS}(A, M, patches)$
/* Step 3: Construct etree via patch-guided nested dissection */
3: $etree \leftarrow \text{BUILDEETREE}(G, gmap, nd_level)$
/* Step 4: Assemble a global permutation from the tree */
4: $perm \leftarrow \text{COMPUTEPerm}(etree, G)$

```
- 

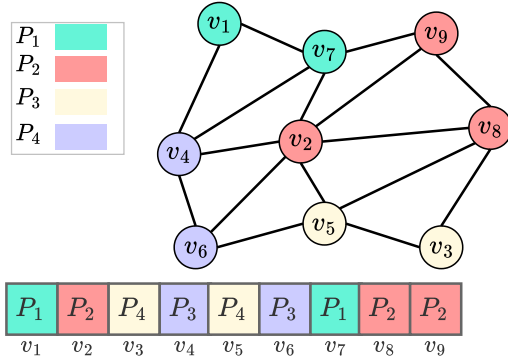


Fig. 6. **Mapping transformation.** The patching algorithm assigns mesh vertices to patches ( $P_1 \dots P_4$ ), from which we construct the group map ( $gmap$ ).

generates the *etree* as part of the permutation process, eliminating a costly step in the symbolic Cholesky phase. Together, our algorithm reduces preprocessing overhead and translates directly into faster end-to-end sparse direct solves.

*Inputs and outputs.* Our algorithm inputs a sparse symmetric positive semidefinite system matrix  $A$ , a mesh  $M$ , and a nested-dissection depth parameter  $nd\_level$ . It outputs a fill-reducing permutation vector  $perm$  and the corresponding *etree*. We use the mesh only to generate patches and the associated quotient graph. Thus, if the patch partition is provided, the mesh input is unnecessary.

## 4.1 Patching and Constructing the Group Map

Our algorithm (Algorithm 1) starts with a preprocessing stage. It includes generating mesh patches and constructing the group map, providing a coarse structure that reduces the separator search space.

*Step 1: Patch computation.* Many graphics applications compute patch-like partitions (e.g., for remeshing, clustering, or domain decomposition) which we can use directly. Otherwise, we compute *patches* using a fast parallel routine. Our implementation uses the GPU patching method from RXMesh [Mahmoud et al. 2021].

*Step 2: Lift patches to the matrix graph.* We construct the graph of  $A$  (without diagonal entries) as  $G = (V_G, E_G)$  and build a group map ( $gmap : V_G \rightarrow \{1, \dots, |patches|\}$ ) by lifting the mesh partition to the graph. In the scalar case, each mesh vertex maps to one graph vertex. In the block case, each mesh vertex maps to a small number of block of graph vertices, in which case we map all graph vertices in the block to the same patch. This covers both scalar Laplacian systems and block-structured Hessians. Figure 6 shows an instance of the scalar case. We use the resulting vertex-to-patch assignment to group the vertices of  $G$ . The map  $gmap$  then assigns each vertex in  $G$  to its corresponding group.

## 4.2 Building the Elimination Tree

Beyond producing a fill-reducing permutation, we construct and expose the *etree*, which encodes Cholesky elimination dependencies and enables scheduling that trades locality for parallelism (§5). High-performance solvers (e.g., cuDSS) use the *etree* to drive parallel numeric execution, and exposing it allows our permutation to integrate into such pipelines.

*Step 3: Patch-guided nested dissection.* Given the matrix graph  $G$  and the group map  $gmap$ , we recursively apply nested dissection for  $nd\_level$  levels while simultaneously constructing the *etree* (Figure 7). At each recursion, we compute a separator set  $s$ , partition the current subgraph into left and right sub-graphs  $g_l$  and  $g_r$ , store the separator at the current tree node, and recurse on the two children. The recursion terminates when the depth reaches zero, at which point the leaf stores the remaining vertices. We represent the *etree* as a binary tree stored in a 1D array (node index  $idx$ , children  $2idx + 1$  and  $2idx + 2$ ). In practice, moderate depths (e.g., 9–10) provide sufficient parallelism [NVIDIA Corporation 2025]. While this procedure mirrors classical nested dissection, our runtime improves by targeting a dominant cost, i.e., separator computation at the top levels

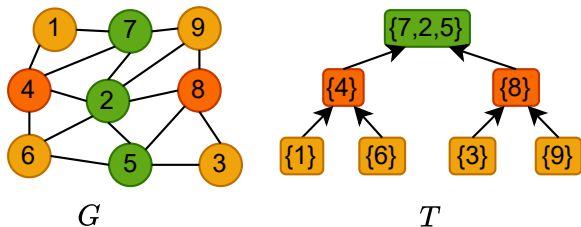


Fig. 7. **Elimination tree construction.** We compute the root separator  $\{7, 2, 5\}$ . For the resulting subgraphs  $g_\ell = \{1, 4, 6\}$  and  $g_r = \{3, 8, 9\}$ , we recurse to compute the next-level separators (e.g.,  $\{4\}$  and  $\{8\}$ ), continuing until reaching the desired depth. We store the full binary tree in a 1D array.

---

#### Algorithm 2 GETSEPARATOR (called by BUILDETREE).

---

**Input:**  $g, gmap$

**Output:**  $s, g_\ell, g_r$

- ```

/* 1) Build quotient graph over patch groups */
1:  $q \leftarrow \text{QUOTIENTGRAPH}(g, gmap)$ 
/* 2) Bipartition the quotient graph (with balance constraint) */
2:  $part_q \leftarrow \text{BIPARTITION}(q)$ 
/* 3) Lift partition and form a separator superset on  $g$  */
3:  $super\_s \leftarrow \text{SUPERSEPARATOR}(g, gmap, part_q)$ 
/* 4) Refine the superset (balance + local refinement) */
4:  $s \leftarrow \text{REFINESEPARATOR}(g, super\_s, gmap, part_q)$ 
/* 5) Induce left/right subgraphs for the next recursion level */
5:  $(g_\ell, g_r) \leftarrow \text{LEFTRIGHT}(g, s, gmap, part_q)$ 

```
-

where subgraphs are largest and separators are most expensive as we discuss next.

Computing separators (GETSEPARATOR). Our key idea is to reuse patch structure when extracting separators. Unlike classical multi-level nested dissection, we (i) operate at the patch granularity using a quotient graph, rather than building a coarsening hierarchy, and (ii) reuse the same patches across all recursion levels, trading some ordering quality for lower permutation overhead.

Algorithm 2 builds the quotient graph q from the current patch group, bipartitions q , and lifts back to vertices in $V(g)$ to form a separator *superset* of boundary vertices. We then refine this superset to reduce its size while maintaining balance, and extract the left and right subgraphs for recursion. Figure 5 illustrates this pipeline.

4.3 Permutation computation

Step 4: Local orderings & concatenation. Given the *etree*, we compute the final permutation in two stages (Algorithm 3). At each tree node, we compute a *local* ordering of its vertices (e.g., using AMD on the induced subgraph) and cache the result. Then, we concatenate these local orderings following a user-selected traversal of the *etree* which we call the *schedule*. §5 explains the role of this order and the flexibility it provides for accelerating the numerical phase.

5 Implementation Details

If the user supplies a grouping of vertices (patches) such that each group induces a connected subgraph in the matrix graph, our method

Algorithm 3 COMPUTEPerm: local orderings and concatenation.

Input: *etree*, g , *schedule*

Output: *perm*

- ```

/* 1) Compute local permutations per tree node */
1: for idx in $[0, \dots, |etree| - 1]$ do
2: $g_{idx} \leftarrow \text{INDUCEDSUBGRAPH}(g, etree[idx].nodes)$
3: $etree[idx].perm_local \leftarrow \text{LOCALORDER}(g_{idx})$
4: end for
/* 2) Concatenate to form global permutation */
5: $perm \leftarrow []$
6: for idx in $schedule(etree)$ do
7: $perm.APPEND(etree[idx].perm_local)$
8: end for

```
- 

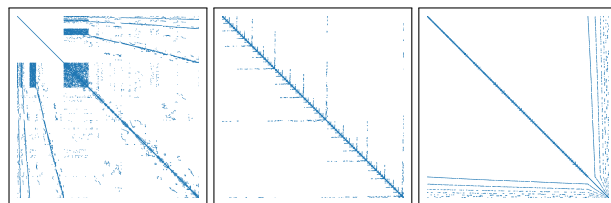


Fig. 8. For the same input (left), different schedules for traversing the elimination tree produce different permutations. Shown are post-order traversal (middle) and level-order traversal (right), which both result in the same fill-in.

consumes it as the *gmap* and proceeds with Steps 3–4. If the provided groups are not connected, the algorithm still runs, but permutation quality can degrade since disconnected groups restrict GETSEPARATOR and typically produce larger and less balanced separators. See Supplemental Materials B for more information about how the quality of patching correlates with separator size and runtime.

*Quotient graph computation.* The quotient graph must be updated at each elimination tree node to produce a valid bipartition. However, a key cost we aim to avoid, especially for large matrices, is repeatedly scanning the full matrix. Since constructing the quotient graph from scratch typically requires reading the entire matrix, we instead build the quotient graph once and then update only node weights and edge weights as we compute *etree* nodes from the root to the leaves. More specifically, we adjust the quotient graph node weights by removing the weight of the (already marked) separators, and adjust the edge weights by removing the edges of the separator nodes.

*Separator set computation.* In separator set computation, we first use the quotient graph and METIS to find a bipartition. This step is fast because quotient graphs are relatively small compared to matrix  $A$ . Next, we obtain a superset of the separator by mapping the nodes in  $V_G$  to the two partitions using their corresponding quotient nodes. This step is the bottleneck of our computation. Finally, we apply METIS’s node refinement strategy to refine the separator. After finding the separator, we remove the separator nodes’ effects from the quotient graph so that it can be reused in consecutive recursive calls of nested dissection. See Supplemental Materials B for more implementation details about separator refinement.

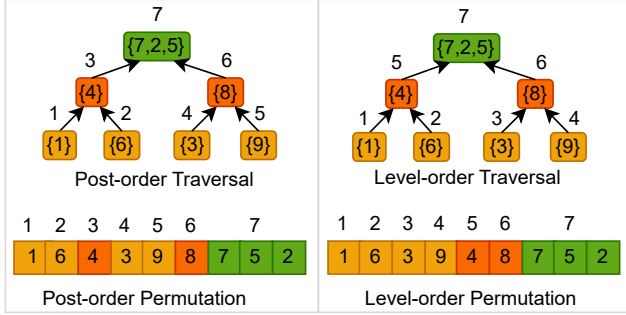


Fig. 9. Permutation vectors from post-order (left) and level-order (right) traversals of the *etree*. Both yield the same fill-in, but can differ in performance due to memory access and parallelism.

*Concatenation and schedules.* After computing the elimination tree, we form the global permutation by concatenating the local permutations associated with tree nodes (Algorithm 3). The primary degree of freedom is the *schedule* used to traverse the elimination tree (Algorithm 3, line 6). A valid schedule must respect elimination dependencies, i.e., no parent can appear before its children. Different valid schedules do not change fill-in but can yield different performance due to locality–parallelism trade-offs. On CPUs, post-order traversal is preferred because it tends to improve temporal locality, i.e., once two sibling subtrees are processed, their results are consumed shortly thereafter by the parent, increasing cache reuse. This is the default in CPU solvers, e.g., CHOLMOD [Chen et al. 2008]. In contrast, GPU solvers often prefer schedules that expose more parallelism, e.g., cuDSS follows a wavefront (level-based) schedule in which nodes are processed level by level starting from the leaves (see Figure 8).

Our implementation provides both post-order and level-order schedules (Figure 9). More generally, the index sequence used in line 6 of Algorithm 3 can be any valid schedule. Note that some CPU solvers (e.g., CHOLMOD) don’t expose a user-defined schedule. Instead, they construct an internal execution order after *etree* construction and then apply the given permutation. In such cases, providing an invalid schedule won’t cause a runtime failure but can degrade performance if separators are assembled before their children. In contrast, cuDSS requires a schedule consistent with its execution model (i.e., a level-order/wavefront schedule); using an incompatible schedule can lead to runtime failure.

## 6 Evaluation

To evaluate the performance impact of our permutation algorithm and its portability across solvers and hardware platforms, we integrate it into two vendor-maintained sparse Cholesky solvers, i.e., NVIDIA cuDSS and Intel MKL. In both, we replace their fill-reducing permutation stage with ours. For cuDSS, we also replace the elimination-tree construction. Subsequent numerical factorization and solve routines are left unchanged, isolating the effect of our permutation on end-to-end performance. We experiment on a system with an Intel Xeon Gold 6248 CPU (20 cores, 2.5 GHz, 28 MB LLC, 202 GB RAM) and an NVIDIA RTX 3080 GPU. We

Table 1. **Application Speedup Summary.** We consider applications under (i) fixed and changing numerical factorization (F1: fixed, F2: changing), and (ii) different right-hand-side (RHS) use patterns (R1: repeated RHS solves, R2: matrix RHS). *Mesh size* denotes the number of mesh vertices. *#iter* is the iteration at which we report the total solve speedup (e.g., for R1+F2 it counts refactorizations with the same sparsity). *max #iter* is the estimated break-even iteration count beyond which the default cuDSS ordering (METIS) becomes faster, if the lower-quality ordering reduces factorization and RHS-solve performance.

| App              | Setting | Mesh size | #iter | speedup | max #iter |
|------------------|---------|-----------|-------|---------|-----------|
| Data Smoothing   | F1,R1   | 1M        | 1     | 5.23x   | —         |
| Data Smoothing   | F1,R1   | 0.1M      | 1     | 2.92x   | —         |
| SCP              | F1,R1   | 1.5M      | 32    | 4.16x   | 108859    |
| SCP              | F1,R1   | 0.16M     | 32    | 2.34x   | inf       |
| Mesh Smoothing   | F2,R2   | 1.76M     | 6     | 3.70x   | 160       |
| Mesh Smoothing   | F2,R2   | 0.17M     | 6     | 2.89x   | 148       |
| Parameterization | F2,R1   | 1.1M      | 13    | 1.47x   | 53        |
| Parameterization | F2,R1   | 0.32M     | 24    | 1.69x   | 167       |

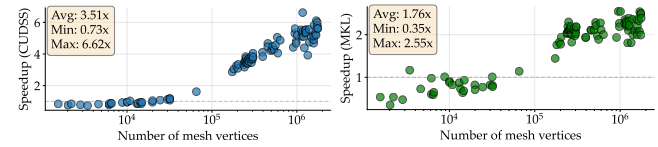


Fig. 10. Speedup of cuDSS (left) and MKL (right) when replacing METIS with our permutation. Averaged across inputs, we achieve on average (geometric mean) 3.51 $\times$  on GPU and 1.76 $\times$  on CPU by reducing permutation overhead while preserving parallel-friendly elimination trees.

use Intel MKL version 2023.4-912 on Ubuntu 24.04 and CUDA 12.7 with cuDSS version 0.7.1. The input meshes we use in these experiments are collected from the Smithsonian [Smithsonian Institution Digitization Program Office 2023], ThreeDScans [Laric 2023], and Thingi10K [Zhou and Jacobson 2016] repositories. We use double precision in all experiments.

Our evaluation proceeds in two parts. We first measure end-to-end solver speedups obtained by integrating our algorithm into cuDSS and Intel MKL across applications. We then study the permutation stage in isolation to identify the sources of these speedups. Together, these experiments capture common usage patterns of sparse Cholesky solvers in graphics applications. Unless otherwise stated, patches are computed on the GPU using Lloyd’s algorithm [Lloyd 1982] with a target patch size of 256 vertices. For comparison, we use METIS version shipped with cuDSS. We use the default parameters for cuDSS, i.e., double precision, complete GPU execution for factorization and solve, and default nested-dissection METIS.

### 6.1 Laplace-Beltrami

We begin with the Laplace-Beltrami operator assembled using libigl’s cotmatrix [Jacobson et al. 2018]. For each mesh, we perform a single sparse Cholesky factorization followed by a solve with a random right-hand side. This workload represents pipelines in which

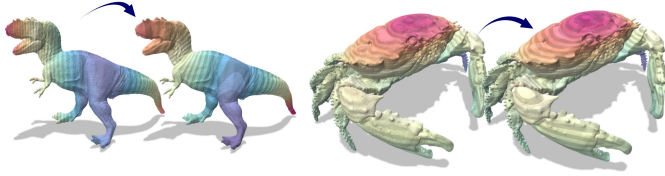


Fig. 11. **Data smoothing via Laplacian regularization.** We recover a smooth scalar function from noisy vertex data by solving a quadratic optimization problem that balances a mass-weighted data term with a Laplacian-based smoothness term.

the system is factorized once and used immediately without amortizing symbolic preprocessing. In this regime, the symbolic phase can dominate runtime with fill-reducing permutation accounting for a large fraction of the cost (Figure 2). To quantify our method’s impact, we integrate it into cuDSS and Intel MKL and measure end-to-end speedups across 103 meshes with 1.5K to 1.8M vertices (Figure 10).

Replacing METIS with our algorithm yields increasing speedups with problem size. For large meshes, reduced permutation overhead directly yields faster solves as permutation increasingly dominates runtime. For meshes larger than 1.5M vertices, we observe speedups of up to 6.62× with cuDSS and 2.55× with Intel MKL. For smaller meshes, the benefits are limited where METIS can perform better since the permutation cost is small (Figure 2). Empirically, our method becomes beneficial above approximately 50K vertices on cuDSS and 100K vertices on Intel MKL. In Supplemental Materials D, we compare against the recently introduced multi-threaded mode in cuDSS—which was released concurrently with our work. In addition, we study the case of refactorizations (i.e., same sparsity with different numerical values) and report the break-even iteration after which our method becomes slower in Supplemental Materials E.

For the remaining evaluation, we focus exclusively on cuDSS since our patching stage is GPU-accelerated, so pairing it with a GPU solver provides a natural end-to-end view. In addition, cuDSS inputs both a permutation and an (*etree*), allowing us to evaluate permutation overhead as well as the quality of the *etree* and its impact on factorization and solve performance.

## 6.2 Data Smoothing

Data smoothing on triangle mesh recovers a smooth scalar function  $x \in \mathbb{R}^{|V_M|}$  from a noisy signal  $y$  defined on the mesh vertices (Figure 11). We compute  $x$  by minimizing a quadratic energy that balances data fidelity and smoothness using Dirichlet energy:  $\min_x (x - y)^T M (x - y) + \alpha x^T L^T M^{-1} L x$ , where  $M$  is the lumped mass matrix,  $L$  is the cotangent Laplacian, and  $\alpha > 0$  controls the smoothing. Setting the gradient to zero yields  $((1 - \alpha)M + \alpha L^T M^{-1} L)x = \alpha M y$ , which we solve using Cholesky factorization.

Table 1 reports end-to-end speedups for a large mesh (1M vertices) and a smaller mesh (100K vertices). We achieve 5.23× and 2.92× speedup on the 1M-vertex mesh and 100K-vertex mesh, respectively. This mirrors the trend in the Laplace-Beltrami evaluation (§6.1), since both involve a single sparse Cholesky factorization where permutation cost dominates at larger sizes.

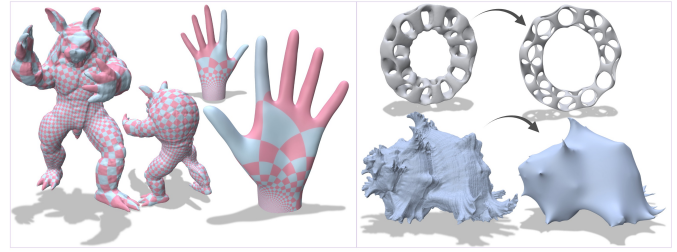


Fig. 12. Results of SCP produced by our implementation (left) and results of six iterations of mesh smoothing applied on a mesh with 1.7M vertices produced by our implementation (right).

## 6.3 Spectral Conformal Parameterization

We next evaluate on spectral conformal parameterization (SCP) [Mullen et al. 2008], a parameterization method that solves a generalized eigenvalue problem derived from the discrete conformal energy (see Figure 12). In practice, SCP is implemented using inverse power iteration, where each iteration solves a sparse linear system with a fixed matrix and different right-hand side. In our implementation, the conformal energy matrix and its sparsity pattern remain fixed. The solver performs a single sparse Cholesky factorization followed by multiple forward/backward substitutions. SCP represents a workload where symbolic analysis and factorization are amortized while permutation quality affect the cost of repeated solves.

We integrate our permutation into cuDSS and measure end-to-end speedup using 32 power iterations. Table 1 shows that replacing METIS leads to 4.16× and 2.34× on the larger and small mesh, respectively. Since forward and backward substitution incur much lower overhead than factorization, accelerating permutation and symbolic preprocessing has a lasting impact when many solves are performed. For smaller meshes, our permutation can improve solve performance relative to METIS. For larger meshes, the patch-based approximation and local AMD permutation may slightly degrade factor quality and increase substitution cost. This effect is not systematic and depends on the sparsity pattern. We analyze this trade-off in §6.6. Overall, SCP demonstrates a complementary regime to the Laplace-Beltrami experiment where a single factorization is reused across many solves. Reducing permutation overhead still yields end-to-end gains even when factorization is amortized.

## 6.4 Mesh Smoothing

We next consider iterative smoothing via mean-curvature flow [Desbrun et al. 1999] (see Figure 12). Each iteration assembles a new system matrix, followed by sparse Cholesky (re) factorization and a solve. The right-hand side is a dense  $|V_M| \times 3$  matrix which we solve simultaneously. This workload combines repeated factorizations with multiple right-hand-side solves, exhibiting a different balance between permutation, factorization, and substitution costs.

After six iterations, our permutation yields a 3.7× speedup for the large mesh and 2.89× for the small mesh (Table 1). The break-even point (measured in repeated full numerical phases) is 160 iterations for the large mesh and 148 for the small mesh. Although our permutation sometimes can lead to slightly slower factorization and

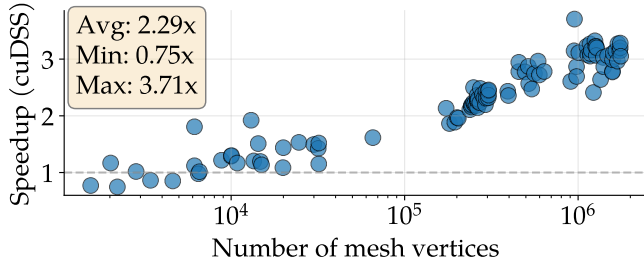


Fig. 13. **End-to-end solver speedup on mesh smoothing.** Using cuDSS, our fill-reducing permutation achieves an average 2.29 $\times$  speedup across six smoothing iterations, with larger meshes benefiting the most.

triangular solves, overall performance still favors our pipeline due to the substantial reduction in the main computational bottleneck, i.e., permutation. Figure 13 shows the end-to-end speedup over cuDSS across different mesh sizes. As seen before, speedup increases with problem size, reaching up to 3.71 $\times$  for the largest meshes.

### 6.5 Symmetric Dirichlet Parameterization

We minimize the symmetric Dirichlet energy [Smith and Schaefer 2015] to compute a low-distortion 2D parameterization of a surface mesh. We solve the resulting nonlinear system using Newton’s method where each iteration assembles and factorizes a sparse Hessian and then solves for a Newton step. This application has similar characteristic to mesh smoothing (§6.4), where matrix numerical values change while the sparsity is constant. Unlike the Laplacian-based workloads in previous sections, this application produces a second-order system. The Hessian sparsity pattern is closely related to the Laplace-Beltrami operator but differs in scale, as each nonzero in the Laplacian corresponds to a dense  $2 \times 2$  Hessian block. Consequently, the Hessian has  $2\times$  as many rows/columns and  $\sim 4\times$  as many nonzeros as the scalar Laplacian.

This increased density makes factorization more expensive, reducing the fraction of end-to-end time spent in permutation. Since sparse Cholesky has complexity  $O\left(\sum_{i=1}^N d(i)^2\right)$  [Lipton et al. 1979], where  $d(i)$  is the number of nonzeros in column  $i$  of the factor  $L$ , replacing scalar entries with  $2 \times 2$  blocks increases the effective column densities by roughly 2. For the 1M-vertex mesh, Laplacian factorization takes 72 ms, while Hessian factorization takes 300 ms. Hence, speedups here are smaller than for mesh smoothing (§6.4), permutation accounts for a larger share of runtime (see Table 1).

Our permutation cost remains comparable to the Laplacian case since we apply it to a compressed graph where we merge each  $2 \times 2$  block into a single node when constructing the matrix graph  $G$ . We expand the resulting permutation and *etree* back to the full Hessian system.

### 6.6 Benchmark and Ablation

We benchmark along two axes: (i) permutation runtime and (ii) fill-in quality. We first compare the permutation time against AMD, METIS, and ParMETIS (Intel oneAPI) to isolate the cost of permutation independent of factorization. We then analyze our algorithm in more detail. First, we study *patch-size sensitivity* by varying the

patch size and measuring fill-in. Second, we present a *module runtime breakdown*, reporting the cost of each stage, including patch construction, patch-based separator computation, and local AMD refinement. Finally, we study *design choices in patch ordering* by comparing runtime and fill-in when (i) replacing patch-based separators with METIS separators and (ii) using AMD vs. METIS for local permutation. These experiments justify our default configuration. We additionally report the speedup of all applications using Intel MKL as a backend in Supplemental Materials F.

*Baseline Comparison.* Figure 14 shows ordering speedups relative to AMD, METIS, and ParMETIS. While our method is less competitive on small problems ( $n < 10^5$ ), it scales substantially better with mesh size by restricting separator search to a smaller quotient graph and reusing patch structure across recursion levels. For  $n > 10^5$ , this yields speedups of up to 10.27 $\times$  over METIS and 2.27 $\times$  over ParMETIS.

*Patch Size Effect.* Figure 15 shows the trade-off induced by patch size. We vary the target patch size in {64, 128, 256} and report (i) runtime breakdowns of each stage in our algorithm and (ii) permutation quality measured by the nonzero ratio  $\text{nnz}(L)/\text{nnz}(A)$ .

Larger patches reduce permutation time by producing fewer patches and a smaller quotient graph, lowering both patch-processing overhead and *etree* construction cost. This is visible in the top plot, where patch sizes 128 and 256 reduce runtime relative to patch size 64, especially on the large mesh. The downside is reduced separator flexibility which can degrade permutation quality and increase fill-in. This is reflected in the bottom plot, where larger patches yield slightly higher  $\text{nnz}(L)/\text{nnz}(A)$  (see Figure 16). We discuss in more details the runtime breakdown of our permutation algorithm in Supplemental Materials G.

The trade-off is most pronounced on the smaller mesh where coarse patches over-constrain separator placement and increase fill-in. In contrast, the large mesh is less sensitive to patch size, as more patches preserve sufficient flexibility. In this regime, a patch size of 256 provides a favorable balance and we use it as the default.

*Patch-based Separator Computation.* A key design choice is to compute separators on the quotient graph rather than on the full matrix graph, reducing separator cost by shrinking the search space and reusing patch structure across recursion levels. We compare our patch-based separator stage (excluding local refinement) against `METIS_ComputeVertexSeparator` [Karypis et al. 2013a] (Figure 17). On the small and large meshes, patch-based computation is 3.22 $\times$  and 3 $\times$  faster, respectively, with 15.44% and 6.07% increases in  $\text{nnz}(L)/\text{nnz}(A)$ . These results show that quotient-graph separators substantially reduce runtime with modest fill-in increases and illustrate how patch size trades off runtime against ordering quality.

*Local Permutation Effect.* Finally, we examine the local permutation used within each *etree* subgraph. We compare AMD (default) against METIS at patch size 256. Figure 18 shows that AMD substantially reduces local-permutation time. On the small and large meshes, AMD is 12.42 $\times$  and 12.74 $\times$  faster, respectively, with 6.67% and 10.78% increases in  $\text{nnz}(L)/\text{nnz}(A)$ . Overall, AMD provides an order-of-magnitude reduction in local ordering time at the cost

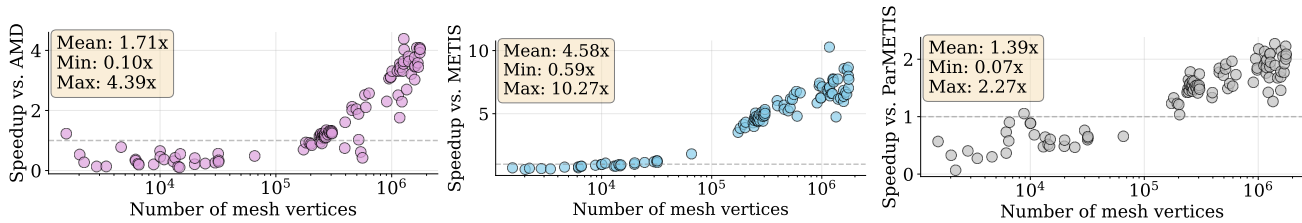


Fig. 14. **Runtime comparison of our algorithm vs. AMD, METIS, and ParMETIS.** Our algorithm scales better than the baseline ordering tools commonly integrated into high-performance linear solvers, and begins to outperform them on meshes with more than 100k vertices.

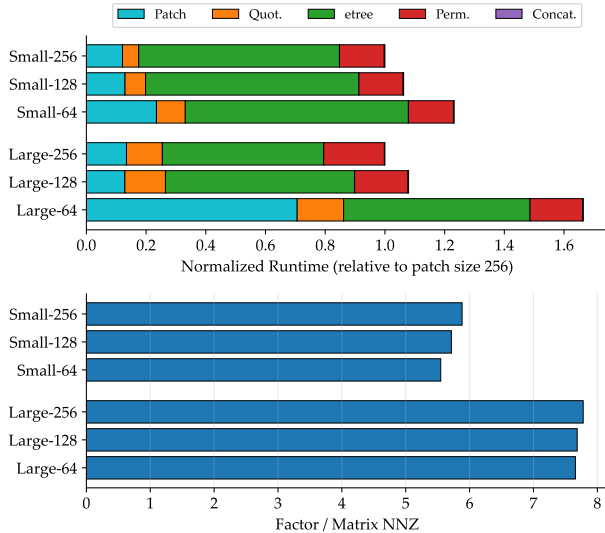


Fig. 15. **Patch size trade-off in our algorithm.** Top: runtime (lower is better) breakdown of each stage (patching, patch-based separator computation, quotient-graph/*etree* construction, and local AMD ordering) for patch sizes 64, 128, 256, shown for a small ( $n \approx 300K$ ) and a large mesh ( $n \approx 1.8M$ ). Each stacked bar is normalized by the total ordering time at patch size 256. Bottom: permutation quality measured by the fill-in ratio  $\text{nnz}(L)/\text{nnz}(A)$  (lower is better). Larger patches reduce permutation time by producing fewer patches and a smaller quotient graph but increase fill-in by restricting separator flexibility. For patch size 256, the total ordering time of our algorithm is 1.717s (large) and 0.207s (small), compared to 10.272s and 1.418s for METIS, respectively.

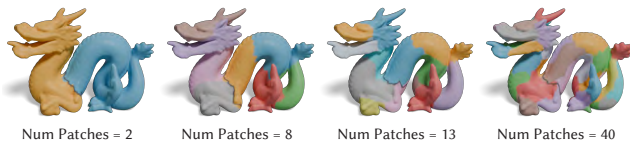


Fig. 16. **Effect of patch size on separator quality.** Decreasing the patch size results in a larger number of patches, allowing our algorithm to produce higher-quality separators, since the separator must follow patch boundaries. However, this comes with a trade-off where increasing the number of patches also increases runtime overhead.

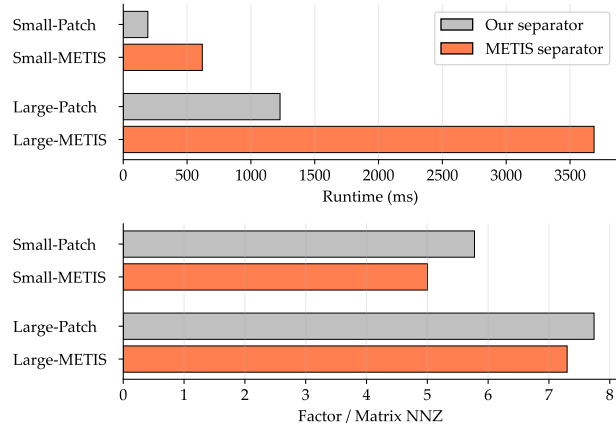


Fig. 17. **Separator computation and separator refinement: METIS vs. our patch-based algorithm.** We compare METIS vertex separator computation and refinement against our algorithm’s patch-based separator stage at patch size 256, on a small mesh and a large mesh. Small-Patch and Small-METIS denote the corresponding method/mesh pair. Top: the patch-based runtime (lower is better) includes patch construction, quotient-graph construction, and *etree* construction (cf. Figure 15). Bottom: permutation quality measured by the fill-in ratio  $\text{nnz}(L)/\text{nnz}(A)$  (lower is better).

of a modest increase in fill-in motivating our default choice when minimizing permutation overhead is the primary objective.

We expand on this ablation in Supplemental Materials H and examine the effect of separator and local permutation on the factorization and triangular-solve runtime.

## 7 Conclusion, Limitations, and Future Works

Sparse Cholesky is the method of choice for solving SPD systems due to its robustness but it scales poorly. We target the main bottleneck in this pipeline, i.e., fill-reducing permutation. We design a simple algorithm for fast matrix permutation with a focus on end-to-end runtime. In doing so, we trade some permutation quality for speed. Our results show this is worthwhile for many use cases, including single solves, repeated solves, and block-structured Hessians.

This trade-off is beneficial when the solve phase is executed only a small number of times before refactorization or a change in matrix structure. In such settings, our method yields a net speedup (§6). However, when the matrix remains fixed and the solve phase is repeated for thousands of iterations, it can cause a small end-to-end slowdown. For example, in inverse rendering, the same factorized

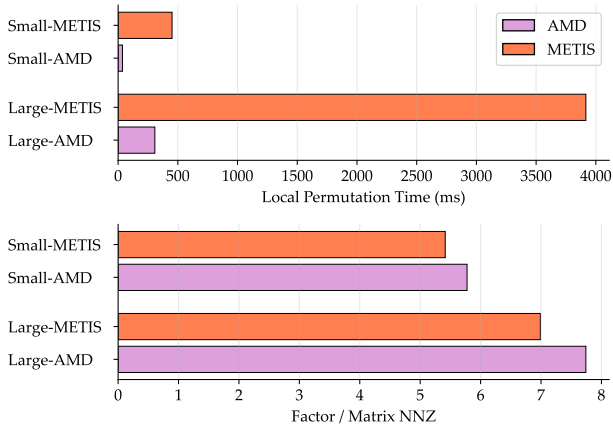


Fig. 18. **Local permutation trade-off: AMD vs. METIS.** Local permutation time (top, lower is better) and fill-in ratio  $\text{nnz}(L)/\text{nnz}(A)$  (bottom, lower is better) for AMD and METIS used as the local permutation step within *etree* construction in our algorithm with patch size 256. AMD yields an order-of-magnitude reduction in local ordering time, at the cost of a modest increase in fill-in.

matrix is reused to solve many right-hand sides (see Supplemental Materials I for details and results).

We achieve this by specializing our algorithm to systems from triangle meshes, where domain structure provides strong guidance for permutation. Extending to other domains is promising, with tetrahedral meshes as a natural next step. In a preliminary tet-mesh experiment using METIS\_KWay for patch generation, our method achieves up to  $3.73\times$  speedup without patching, but drops to  $0.83\times$  when the patching time is included. This indicates that volumetric meshes will require a fast tetrahedral patching routine. Future work also includes GPU-based separator computation and parallel local ordering.

## Acknowledgments

The authors would like to thank Jonathan Ragan-Kelley for valuable discussions. The MIT Geometric Data Processing Group acknowledges the generous support of National Science Foundation grants IIS2335492 and OAC2403239, from the CSAIL Future of Data and FinTechAI programs, from the MIT-IBM Watson AI Laboratory, from the Wistron Corporation, from the MIT Generative AI Impact Consortium, from the Toyota-CSAIL Joint Research Center, and from Schmidt Sciences.

## References

Patrick R. Amestoy, Timothy A. Davis, and Iain S. Duff. 1996. An Approximate Minimum Degree Ordering Algorithm. *SIAM J. Matrix Anal. Appl.* 17, 4 (1996), 886–905. <https://doi.org/10.1137/S0895479894278952>

Apple Inc. 2025. Accelerate Framework. <https://developer.apple.com/documentation/accelerate>.

Saman Ashkiani, Martin Farach-Colton, and John D. Owens. 2018. A Dynamic Hash Table for the GPU. In *Proceedings of the 32nd IEEE International Parallel and Distributed Processing Symposium (IPDPS 2018)*, 419–429. <https://doi.org/10.1109/IPDPS.2018.00052>

Umberto Bertelè and Francesco Brioschi. 1969. A New Algorithm for the Solution of the Secondary Optimization Problem in Non-Serial Dynamic Programming. *J. Math. Anal. Appl.* 27, 3 (Sept. 1969), 565–574. [https://doi.org/10.1016/0022-247x\(69\)90137-1](https://doi.org/10.1016/0022-247x(69)90137-1)

Umberto Bertelè and Francesco Brioschi. 1972. *Nonserial Dynamic Programming*. Academic Press.

Charles-Edmond Bichot and Patrick Siarry. 2013. *Graph partitioning*. John Wiley & Sons.

Yen-Hsiang Chang, Aydın Buluç, and James Demmel. 2025. Parallelizing the Approximate Minimum Degree Ordering Algorithm: Strategies and Evaluation. *arXiv preprint arXiv:2504.17097* (2025).

Yangqing Chen, Timothy A. Davis, William W. Hager, and Sivasankaran Rajamanickam. 2008. Algorithm 887: CHOLMOD, Supernodal Sparse Cholesky Factorization and Update/Downdate. *ACM Trans. Math. Softw.* 35, 3, Article 22 (Oct. 2008), 14 pages. <https://doi.org/10.1145/1391989.1391995>

Kazem Cheshmi, Danny M. Kaufman, Shoab Kamil, and Maryam Mehri Dehnavi. 2020. NASOQ: Numerically Accurate Sparsity-Oriented QP Solver. *ACM Transactions on Graphics* 39, 4 (Aug. 2020), 96:1–96:17. <https://doi.org/10.1145/3386569.3392486>

C. Chevalier and F. Pellegrini. 2008. PT-SCOTCH: A tool for efficient parallel graph ordering. *Parallel Comput.* 34, 6–8 (July 2008), 318–331. <https://doi.org/10.1016/j.parco.2007.12.001>

Robert Cummings, Matthew Fahrback, and Animesh Fatehpuria. 2021. A Fast Minimum Degree Algorithm and Matching Lower Bound. In *Proceedings of the 2021 ACM-SIAM Symposium on Discrete Algorithms (SODA)*. Society for Industrial and Applied Mathematics, 724–734. <https://doi.org/10.1137/1.9781611976465.45>

E. Cuthill and J. McKee. 1969. Reducing the bandwidth of sparse symmetric matrices. In *Proceedings of the 1969 24th National Conference*. Association for Computing Machinery, New York, NY, USA, 157–172. <https://doi.org/10.1145/800195.805928>

Timothy A. Davis. 2006. *Direct Methods for Sparse Linear Systems*. Society for Industrial and Applied Mathematics. <https://doi.org/10.1137/1.9780898718881>

Mathieu Desbrun, Mark Meyer, Peter Schröder, and Alan H. Barr. 1999. Implicit Fairing of Irregular Meshes Using Diffusion and Curvature Flow. In *Proceedings of the 26th Annual Conference on Computer Graphics and Interactive Techniques (SIGGRAPH '99)*. ACM Press/Addison-Wesley Publishing Co., USA, 317–324. <https://doi.org/10.1145/311535.311576>

Alan George. 1973. Nested Dissection of a Regular Finite Element Mesh. *SIAM J. Numer. Anal.* 10, 2 (1973), 345–363. <https://doi.org/10.1137/0710032>

Alan George and Joseph W. H. Liu. 1980. A Fast Implementation of the Minimum Degree Algorithm Using Quotient Graphs. *ACM Trans. Math. Software* 6, 3 (Sept. 1980), 337–358. <https://doi.org/10.1145/355900.355906>

Philipp Herholz and Marc Alexa. 2018. Factor Once: Reusing Cholesky Factorizations on Sub-Meshes. *ACM Transactions on Graphics* 37, 6 (Dec. 2018), 230:1–230:9. <https://doi.org/10.1145/3272127.3275107>

Philipp Herholz and Olga Sorkine-Hornung. 2020. Sparse Cholesky Updates for Interactive Mesh Parameterization. *ACM Transactions on Graphics* 39, 6 (Nov. 2020), 202:1–202:14. <https://doi.org/10.1145/3414685.3417828>

Intel Corporation. 2025. Intel Math Kernel Library (MKL). <https://www.intel.com/content/www/us/en/developer/tools/oneapi/oneapi.html>.

Alec Jacobson, Daniele Panozzo, et al. 2018. libigl: A simple C++ geometry processing library. <https://libigl.github.io/>.

George Karypis et al. 2013a. METIS – Serial Graph Partitioning and Fill-reducing Matrix Ordering. <http://glaros.dtc.umn.edu/gkhome/metis/metis/overview>.

George Karypis et al. 2013b. ParMETIS – Parallel Graph Partitioning and Fill-reducing Matrix Ordering. <http://glaros.dtc.umn.edu/gkhome/metis/parmetis/overview>.

George Karypis and Vipin Kumar. 1998. A Fast and High Quality Multilevel Scheme for Partitioning Irregular Graphs. *SIAM Journal on Scientific Computing* 20, 1 (1998), 359–392. <https://doi.org/10.1137/S1064827595287997>

Oliver Laric. 2023. *Three D Scans*. <https://threedscans.com/>.

Richard J. Lipton, Donald J. Rose, and Robert Endre Tarjan. 1979. Generalized Nested Dissection. *SIAM J. Numer. Anal.* 16, 2 (1979), 346–358. <https://doi.org/10.1137/0716027>

Stuart P. Lloyd. 1982. Least Squares Quantization in PCM. *IEEE Transactions on Information Theory* 28, 2 (March 1982), 129–137. <https://doi.org/10.1109/TIT.1982.1056489>

Ahmed H. Mahmoud, Serban D. Porumbescu, and John D. Owens. 2021. RXMesh: A GPU Mesh Data Structure. *ACM Transactions on Graphics* 40, 4, Article 104 (Aug. 2021), 16 pages. <https://doi.org/10.1145/3450626.3459748>

Patrick Mullen, Yiyang Tong, Pierre Alliez, and Mathieu Desbrun. 2008. Spectral Conformal Parameterization. In *Proceedings of the Symposium on Geometry Processing*. *Computer Graphics Forum*, 1487–1494. <https://doi.org/10.5555/1731309.1731335>

NVIDIA Corporation. 2025. cuDSS: Release 0.7.1. <https://developer.nvidia.com/cudss/>.

Christian Schulz and Darren Strash. 2018. *Graph Partitioning: Formulations and Applications to Big Data*. Springer International Publishing, Cham, 1–7. [https://doi.org/10.1007/978-3-319-63962-8\\_312-2](https://doi.org/10.1007/978-3-319-63962-8_312-2)

Jennifer Scott and Miroslav Tuma. 2023. *Algorithms for Sparse Linear Systems* (1 ed.). Birkhäuser Cham, XIX–242 pages. <https://doi.org/10.1007/978-3-031-25820-6>

Jason Smith and Scott Schaefer. 2015. Bijective Parameterization with Free Boundaries. *ACM Trans. Graph.* 34, 4, Article 70 (July 2015), 9 pages. <https://doi.org/10.1145/2766947>

- Smithsonian Institution Digitization Program Office. 2023. *Smithsonian 3D Digitization*. <https://3d.si.edu/>.
- William F. Tinney and John W. Walker. 1967. Direct solutions of sparse network equations by optimally ordered triangular factorization. *Proc. IEEE* 55, 11 (1967), 1801–1809. <https://doi.org/10.1109/PROC.1967.6011>
- Mihalis Yannakakis. 1981. Computing the Minimum Fill-In is NP-Complete. *SIAM Journal on Algebraic Discrete Methods* 2, 1 (1981), 77–79. <https://doi.org/10.1137/0602010>
- Chang Yu, Yi Xu, Ye Kuang, Yuanming Hu, and Tiantian Liu. 2022. MeshTaichi: A Compiler for Efficient Mesh-based Operations. *ACM Transactions on Graphics* 41, 6, Article 252 (Nov. 2022), 17 pages. <https://doi.org/10.1145/3550454.3555430>
- Behrooz Zarebavani, Danny M. Kaufman, David I. W. Levin, and Maryam Mehri Dehnavi. 2025. Adaptive Algebraic Reuse of Reordering in Cholesky Factorizations with Dynamic Sparsity Patterns. *ACM Transactions on Graphics* 44, 4 (July 2025), 119:1–119:17. <https://doi.org/10.1145/3731179>
- Qingnan Zhou and Alec Jacobson. 2016. Thingi10K: A Dataset of 10,000 3D-Printing Models. *CoRR* (May 2016). arXiv:cs.GR/1605.04797

# Fast Sparse Matrix Permutation for Mesh-Based Direct Solvers – Supplemental Materials

BEHROOZ ZAREBAVANI\*, University of Toronto, Canada

AHMED H. MAHMOUD\*, Massachusetts Institute of Technology, USA

ANA DODIK, Massachusetts Institute of Technology, USA

CHANGCHENG YUAN, Texas A&M University, USA

SERBAN D. PORUMBESCU, University of California, Davis, USA

JOHN D. OWENS, University of California, Davis, USA

MARYAM MEHRI DEHNAVI†, University of Toronto, Canada and NVIDIA Research, USA

JUSTIN SOLOMON†, Massachusetts Institute of Technology, USA

## A Parallel Sparse Triangular Solvers

To better understand the desirable properties of a symmetric permutation  $PAP^t$ , we consider the effect of the permutation on the fill-in of the Cholesky factor and the solve time. A symmetric permutation  $PAP^t$  is equivalent to renaming the nodes of the graph  $G$  of  $A$ . Figure 1 compares three orderings of a Laplace-Beltrami matrix, i.e., (i) the random input permutation, (ii) a minimum-degree ordering, and (iii) a nested-dissection ordering.

Case (i) incurs high fill, motivating the need for a fill-reducing permutation. Cases (ii) and (iii) both yield low fill and factors of equal size, but their elimination trees differ, where (iii) has a shorter critical path and thus exposes more parallelism during the solve.

In (ii), the elimination tree forms a chain, so the forward solve must proceed strictly sequentially, i.e., each unknown depends on the previously computed ones. In contrast, in (iii) the elimination tree splits into two independent subtrees  $\{1, 2\}$  and  $\{3, 4\}$ . These subtrees can be solved concurrently on separate threads since there are no dependencies between them. The final variable,  $x_5$ , corresponds to the separator node that connects the two subgraphs, and is computed only after both subtrees finish. This structure, induced by nested dissection, makes the solve well-suited for parallel execution.

\*Joint first author

†Joint last author

Authors' Contact Information: Behrooz Zarebavani, Department of Computer Science, University of Toronto, Toronto, ON, Canada, behrooz.zarebavani@gmail.com; Ahmed H. Mahmoud, Computer Science & Artificial Intelligence Laboratory, Massachusetts Institute of Technology, Cambridge, MA, USA, ahdhn@mit.edu; Ana Dodik, Computer Science & Artificial Intelligence Laboratory, Massachusetts Institute of Technology, Cambridge, MA, USA, anadodik@mit.edu; Changcheng Yuan, Department of Computer Science and Engineering, Texas A&M University, College Station, TX, USA, eric.yuan.cc@gmail.com; Serban D. Porumbescu, Department of Electrical and Computer Engineering, University of California, Davis, Davis, CA, USA, sdporumbescu@ucdavis.edu; John D. Owens, Department of Electrical and Computer Engineering, University of California, Davis, Davis, CA, USA, jowens@ece.ucdavis.edu; Maryam Mehri Dehnavi, Department of Computer Science, University of Toronto, Toronto, ON, Canada, mmehride@cs.toronto.edu and NVIDIA Research, USA, mdehnavi@nvidia.com; Justin Solomon, Computer Science & Artificial Intelligence Laboratory, Massachusetts Institute of Technology, Cambridge, MA, USA, jsolomon@mit.edu.



This work is licensed under a Creative Commons Attribution 4.0 International License. SIGGRAPH Conference Papers '26, Los Angeles, CA, USA © 2026 Copyright held by the owner/author(s). ACM ISBN 979-8-4007-2554-8/2026/07 https://doi.org/10.1145/3799902.3811189

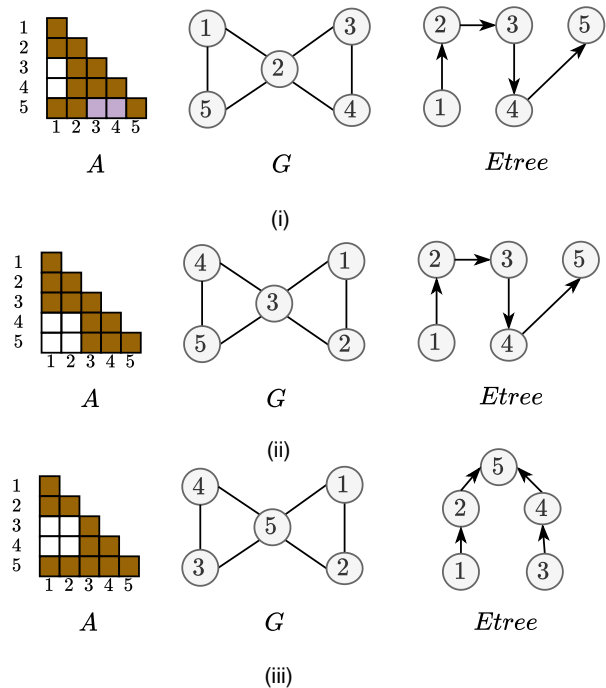


Fig. 1. **Effect of ordering on fill-in, etree, and solver parallelism.** Three symmetric orderings of the same matrix  $A$ : (i) the input ordering incurs high fill (purple cells); (ii) a minimum-degree ordering is fill-free but produces a chain *etree*, forcing a fully serial numerical phase; (iii) a nested-dissection ordering is also fill-free but places the separator vertex last, yielding two independent subtrees  $\{1, 2\}$  and  $\{3, 4\}$  that can be solved in parallel before the root.

## B Patch Clustering Quality, Separator Size, and Runtime

*Clustering-quality metrics.* We measure patch quality with two standard graph-clustering quantities. The *edge-cut ratio* ( $\kappa$ ) is the fraction of edges in the matrix graph whose two endpoints lie in different patches. The *boundary ratio* ( $\beta$ ) is the average fraction of a patch's vertices that touch another patch. Formally, for patches  $\{P_i\}_{i=1}^{|P|}$  on the matrix graph  $G = (V, E)$  with assignment  $c : V \rightarrow$

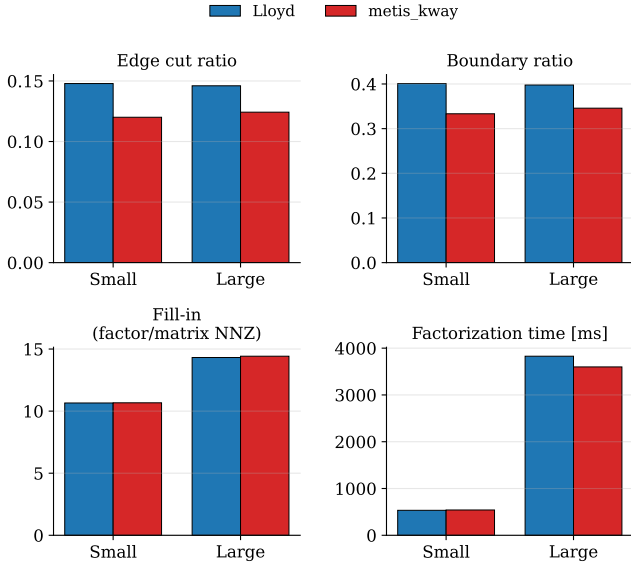


Fig. 2. **Patch clustering quality vs. downstream cost at fixed patch size (256).** Our default Lloyd-based patching vs. METIS  $k$ -way on a small and a large mesh. Factorization time here only includes the time for the factorization step without the permutation computation. METIS  $k$ -way produces tighter clusters (lower  $\kappa$  and  $\beta$ ) at essentially unchanged fill-in, yet factorization time drops slightly.

$\{1, \dots, |\mathcal{P}|\}$ ,

$$\kappa = \frac{|\{(u, v) \in E : c(u) \neq c(v)\}|}{|E|}, \quad \beta = \frac{1}{|\mathcal{P}|} \sum_{i=1}^{|\mathcal{P}|} \frac{|\partial P_i|}{|P_i|},$$

where  $\partial P_i = \{v \in P_i : \exists u \in \Gamma_G(v), c(u) \neq i\}$ . Both metrics directly bound the separator size since  $S^+ = \bigcup_i \partial P_i$ , where  $S^+$  is the separator superset (see Supplemental Materials C). Thus, smaller  $\kappa$  and  $\beta$  should lead to a smaller starting set for the refinement algorithm and hence a smaller refined separator  $S^*$ .

**Patch size.** Patch size is the first knob on  $\kappa$  and  $\beta$  that we use to trade runtime overhead for separator quality. Larger patches shrink the quotient graph and reduce fill-reducing overhead but they also grow patch boundaries and so enlarge  $|S^+|$ ,  $|S^*|$ , fill-in, and factorization cost (Figure 13). This is the mechanism behind the 15.44% and 6.07% fill-in increases of our patch-based separator over METIS\_ComputeVertexSeparator in §6.6, which translate into the 22% and 10% factorization-time increases shown in Figure 6 on the small and large meshes.

**Patch quality at fixed patch size.** Figure 2 compares our default Lloyd-based patching against METIS  $k$ -way partitions at patch size 256 on the same small and large mesh pair used throughout the ablation. METIS  $k$ -way produces lower  $\kappa$  and lower  $\beta$  on both meshes (top) but the fill-in ratio  $\text{nnz}(L)/\text{nnz}(A)$  is essentially indistinguishable between the two patching methods (bottom left). Factorization time is slightly lower for the higher-quality METIS  $k$ -way clustering (bottom right). Due to more uniform clusters, nested-dissection

produces a more balanced elimination tree and hence a more uniform parallel work distribution in Cholesky factorization. Therefore, higher-quality clustering lowers factorization time even when the factor is the same size. Note that Lloyd patching is an order of magnitude faster than METIS  $k$ -way, e.g., on a mesh with 1.7M vertices, METIS  $k$ -way takes 14.1 seconds while Lloyd takes 0.41 seconds, i.e., 34.4× faster. This is the main reason we use Lloyd patching as our default, since the downstream factorization time increase is modest compared to the clustering time reduction.

### C Separator Refinement

Here, we expand on the SUPERSEPARATOR and REFINESEPARATOR steps of Algorithm 2 which together turn a bipartition of the quotient graph into a vertex separator on the full subgraph.

*From a quotient bipartition to a separator superset.* Given the current subgraph  $g = (V_g, E_g)$  and the patch map  $gmap : V_g \rightarrow V_q$ , METIS bipartitions the quotient graph  $q$  into  $V_q = A_q \cup B_q$ , producing  $part_q : V_q \rightarrow \{A, B\}$ . We *lift* this bipartition to the matrix graph by assigning every vertex to the side of its patch,  $part(v) = part_q(gmap(v))$ . Since the quotient bipartition is patch-level, no individual vertex is yet flagged as a separator. The *separator superset*  $S^+$  is then the set of patch-boundary vertices in  $V_g$ :

$$S^+ = \{v \in V_g : \exists u \in \text{Neighbors}(v) \text{ with } part(u) \neq part(v)\}.$$

Removing  $S^+$  from  $g$  disconnects the two sides. Thus,  $S^+$  is a valid, albeit, oversized vertex separator where only a small subset of the boundary is actually needed to disconnect  $A$  from  $B$ .

*Refining the separator superset.* We pass  $(g, S^+, part)$  to METIS’s node-based Fiduccia–Mattheyses (FM) refinement [Karypis et al. 2013; Karypis and Kumar 1998]. Two priority queues (one per side) are initialized with all  $v \in S^+$ , keyed by the gain of moving  $v$  out of the separator into side  $X \in \{A, B\}$ ,

$$\text{gain}(v \rightarrow A) = \eta(v) - \sum_{u \in \Gamma_g(v) \cap B} \eta(u),$$

where  $\eta(\cdot)$  is the vertex weight (the gain to  $B$  is symmetric). Intuitively, moving  $v$  to  $A$  shrinks  $S$  by  $\eta(v)$  but forces every  $B$ -neighbor of  $v$  to join  $S$ , so the gain is the net change in separator weight and is positive only when  $v$  has fewer (or lighter) neighbors on the opposite side than its own weight. At each step, the algorithm pops the highest-gain vertex, biased toward the *lighter* side whenever the running partition weights would otherwise exceed the balance tolerance, moves it out of  $S$ , and pulls any neighbor on the opposite side into  $S$  so that the separator remains valid. Newly added separator vertices are inserted into the queues with gains recomputed on the current partition.

A pass terminates when both queues are empty or after a fixed number of non-improving moves. The smallest balanced separator  $S^*$  observed during the pass is then restored, making the procedure monotone in  $|S|$ . Multiple passes are run until no further reduction is possible. The output  $s = S^*$  is the refined separator stored at the current *etree* node.

### D Comparison against Multi-threaded Mode in cuDSS

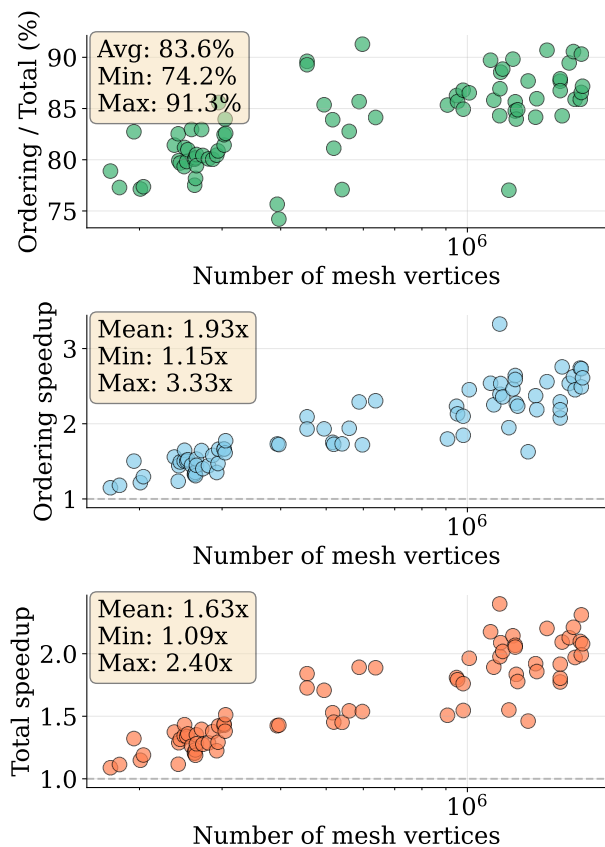


Fig. 3. **Comparison against cuDSS MT-mode (parallel METIS).** For meshes with more than 50k vertices from the suite of §6.1, we report (top) the share of cuDSS single-solve time spent in fill-reducing ordering when MT-mode is enabled; (middle) the ordering-stage speedup of our patch-based permutation over cuDSS MT-METIS; and (bottom) the end-to-end Laplace–Beltrami speedup over cuDSS with MT-mode ordering.

Our algorithm uses a serial METIS implementation in its elimination-tree pipeline. To be fully comprehensive, we additionally compare against the newly-added multi-threaded (MT) mode in cuDSS that allows for CPU-parallel METIS implementation. We reuse the hardware and software setup of §6 and the 103-mesh Laplace–Beltrami suite of §6.1—restricted to meshes with more than 50k vertices. Below this size, patching and decomposition-tree construction dominate and exceed the cost of the METIS baseline, so the comparison is only meaningful at scale (see §6.1). Figure 3 shows the bottleneck breakdown, the ordering-stage speedup, and the end-to-end application speedup of our algorithm vs. cuDSS with MT mode.

*Bottleneck.* Enabling MT-mode does not change which stage dominates cuDSS. Figure 3 (top) shows that fill-reducing ordering still accounts for 83.6% of single-solve time on average. The analysis phase remains the dominant cost even when METIS is run in parallel.

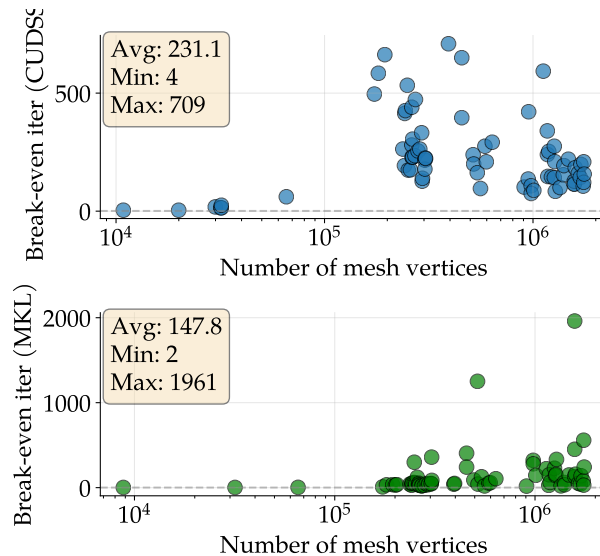


Fig. 4. **Break-even iteration for Laplace–Beltrami.** The distribution of break-even iteration counts on cuDSS and MKL across the 103-mesh suite from §6.1.

*Ordering speedup.* Figure 3 (middle) shows the speedup of our patch-based permutation over cuDSS MT-METIS at the ordering stage. We achieve up to 3.33 $\times$  speedup with a mean of 1.93 $\times$  (min 1.15 $\times$ ). Consistent with the trends in §6.1 and Figure 8, the largest gains occur on the largest meshes, confirming that our algorithm scales with problem size even against a multi-threaded baseline.

*End-to-end speedup.* Figure 3 (bottom) shows the end-to-end application speedup over cuDSS with MT-mode ordering. We obtain up to 2.40 $\times$  with a mean of 1.63 $\times$  (min 1.09 $\times$ ), in line with the single-factorization speedups reported throughout §6.

## E Break-even Iteration for Laplace–Beltrami Application

The Laplace–Beltrami experiment in §6.1 is a single-factorization workload in which fill-reducing permutation can dominate run-time. With repeated refactorizations with the same sparsity pattern are performed across different iterations, our permutation’s one-time savings are amortized against any additional factorization/solve overhead introduced by a lower-quality factor (higher  $\text{nnz}(L)/\text{nnz}(A)$ ). For meshes on which this happens, there exists a break-even iteration count beyond which the baseline METIS ordering should be preferred. Figure 4 reports the empirical distribution of this break-even across the 103-mesh suite used in Figure 8.

We classify an input mesh as (i) always competitive (our permutation is never slower than METIS), (ii) already slower at iteration 1, or (iii) faster at iteration 1 but eventually crossed by METIS after a finite number of refactorizations. With cuDSS, 13% of the 103 meshes are always competitive, 15% are already slower than METIS at iteration 1, and the remaining 73% are faster at iteration 1 and are only crossed by METIS after a finite number of refactorizations. The MKL breakdown (100 meshes) is similar but shifted; 7% always

Table 1. **Application speedup with Intel MKL.** Similar to Table 1, we consider applications under (i) fixed and changing numerical factorization (F1: fixed, F2: changing), and (ii) different right-hand-side (RHS) use patterns (R1: repeated RHS solves, R2: matrix RHS). *Mesh size* denotes the number of mesh vertices. *#iter* is the iteration at which we report the total solve speedup. *max #iter* is the estimated break-even iteration count beyond which the default MKL (METIS) ordering becomes faster.

| App              | Setting | Mesh size | #iter | speedup | max #iter |
|------------------|---------|-----------|-------|---------|-----------|
| Data Smoothing   | F1,R1   | 1M        | 2     | 1.55×   | inf       |
| Data Smoothing   | F1,R1   | 0.1M      | 2     | 0.29×   | 1         |
| SCP              | F1,R2   | 1.5M      | 32    | 1.38×   | 321       |
| SCP              | F1,R2   | 0.16M     | 32    | 1.15×   | 93        |
| Mesh Smoothing   | F2,R2   | 1.76M     | 10    | 1.36×   | 825       |
| Mesh Smoothing   | F2,R2   | 0.17M     | 10    | 0.91×   | 4         |
| Parameterization | F2,R1   | 1.1M      | 13    | 1.12×   | 42        |
| Parameterization | F2,R1   | 0.32M     | 2     | 1.49×   | 56        |

competitive, 22% already slower at iteration 1, and 71% with a finite crossover. In other words, on the single-factorization workload reported in §6.1 our permutation provides an end-to-end speedup on roughly 86% of meshes on cuDSS and 78% on MKL, and a non-trivial subset remains competitive indefinitely. The higher “already slower at iter 1” share on MKL (22% vs. 15%) is consistent with the smaller MKL speedups in Figure 8 (right) and with the mesh-size threshold of approximately 100k vertices reported for MKL in §6.1. Below that threshold, permutation is not the bottleneck (cf. Figure 2) and METIS can already be faster at iteration 1. For the vast majority of meshes, however, the break-even count is large enough that we gain speedup in practice.

## F MKL results for Applications

To complement the cuDSS evaluation in §6, we also report the timings of all applications with Intel MKL as the backend. Similar to the evaluation with cuDSS (§6), we replace the fill-reducing permutation stage of MKL with our algorithm while leaving numerical factorization and solve routines unchanged to isolate the effect of our permutation on end-to-end performance. The Laplace–Beltrami experiment speedup on MKL is reported in Figure 8 (right) and discussed in §6.1. Table 1 reports the remaining application results.

## G Permutation Runtime Breakdown

In our pipeline, we perform the symbolic analysis once for each input mesh in each application. Thus, the relative cost of each ordering stage (i.e., patch generation, separator calculation, quotient-graph/*etree* construction, and local permutation) is determined by the sparsity pattern of the input matrix/mesh rather than by the downstream solve loop. For a Laplacian-like sparsity, Figure 12 shows the runtime breakdown on a representative small and large mesh. The same breakdown follows for most of the applications (Mesh Smoothing, Data Smoothing, and Spectral Conformal Parameterization) since they all rely on the Laplacian-like sparsity.

Here we focus on the symmetric Dirichlet parameterization (§6.5) whose Hessian exhibits a  $2 \times 2$  block structure. Figure 5 shows

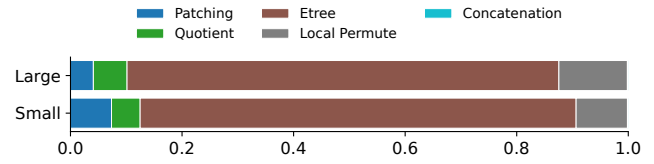


Fig. 5. **Permutation runtime breakdown for Hessian-like sparsity.** Stacked runtime breakdown of each stage of our algorithm on the Hessian matrix which has a  $2 \times 2$  dense-block structure on a small (0.3k faces) and a large (1.1M faces) mesh. Since we order a compressed scalar graph that is structurally equivalent to a Laplacian, the per-phase profile closely matches Figure 12. The additional block expansion stage (part of the Concatenation) contributes a negligible share of the total runtime.

that the per-phase profile on the Hessian-like sparsity follows the same trend as the Laplacian profile of Figure 12. This is because (as described in §6.5) we first compress the input by merging each pair of consecutive rows/columns (the two entries of a  $2 \times 2$  Hessian block) into a single graph vertex, yielding a scalar graph. This operation is trivial and does not take time. All subsequent permutation stages (i.e., patch generation, separator calculation, quotient-graph/*etree* construction, and local permutation) operate on this compressed graph. Thus, their runtimes track the Laplacian-like sparsity case up to a small constant factor due to the slightly different edge weights.

Additionally, after the compressed graph permutation, each permuted vertex  $X$  is expanded to the two consecutive Hessian indices  $2X$  and  $2X+1$ . We call this *block expansion*. Since the two rows/columns inside a  $2 \times 2$  block form a clique in the full Hessian graph, any valid elimination order must number them consecutively and numbering them in the pair  $(2X, 2X+1)$  is therefore optimal. The expansion is a single linear-time pass over the permutation and *etree* (part of the Concatenation stage). Thus, it contributes a negligible share of the total ordering runtime as shown in Figure 5.

## H Extended Ablation of Separator Computation and Local Permutation Effect

Figures 14 and 15 show the permutation time and the fill-in ratio for the separator and local-permutation ablations of §6.6. The fill-in ratio is a proxy for factor quality. However, the downstream cost/time is the combined numerical factorization and triangular-solve time. Here, we ablate those runtimes using the same configurations and meshes as Figures 14 and Figure 15. Figure 6 shows the separator-stage ablation and Figure 7 shows the local-permutation ablation.

*Separator runtime effect.* On the large mesh, the 6.07% increase in fill-in ratio reported in §6.6 translates into 10% increase in factorization time and 2% increase in triangular-solve time which shows that separator quality impacts factorization runtime more than the solve runtime. Similar trend can be seen for the smaller mesh where the 15.44% fill-in increase yields a 22% increase in factorization/solve overhead. Overall, since the increase in fill-in is minimal, the impact on factorization and triangular-solve runtime is also minimal.

*Local permutation runtime effect.* On the large mesh, combining our patch-based nested-dissection separators with AMD as the local-permutation step yields factorization and triangular-solve runtime

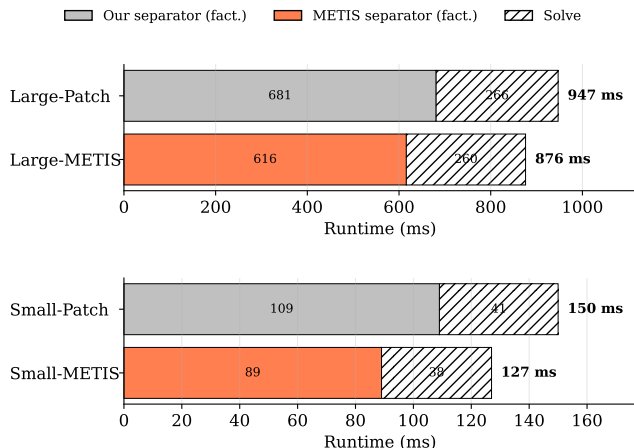


Fig. 6. **Separator computation runtime effect: METIS vs. patch-based.** Factorization (top) and triangular-solve (bottom) time when computing separators with `METIS_ComputeVertexSeparator` versus our patch-based separator stage at patch size 256, on a small mesh and a large mesh. Labels such as `Small-Patch` and `Small-METIS` denote the corresponding method/mesh pair. Factorization here does not include the permutation time. Complements Figure 14.

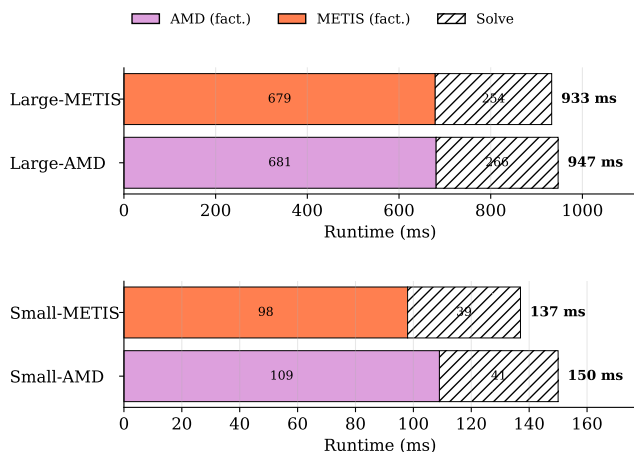


Fig. 7. **Local permutation runtime effect: AMD vs. METIS.** Factorization (top) and triangular-solve (bottom) time when using AMD or METIS as the local permutation step within each *etree* subgraph (patch size 256), on a small mesh and a large mesh. Factorization here does not include the permutation time. Complements Figure 15.

that is essentially on par with using METIS (nested dissection) as the local step as well, i.e., the order-of-magnitude local-permutation speedup of AMD over METIS reported in §6.6 comes with effectively no runtime penalty downstream.

## I Inverse Rendering

We additionally evaluate our permutation on a inverse rendering application based on inverse rendering [Nicolet et al. 2021]. In this

Table 2. **Inverse rendering speedup.** Per-remesh-level results of inverse rendering on the Nefertiti mesh from Nicolet et al. [2021]. *Mesh size* is the number of vertices at that remesh level, *#iter* is the iteration at which the total solve speedup is reported, and *max #iter* is the estimated break-even iteration count beyond which the default cuDSS (i.e., METIS) ordering becomes faster.

| Mesh size | #iter | speedup | max #iter |
|-----------|-------|---------|-----------|
| 0.056M    | 4001  | 0.68×   | 106       |
| 0.18M     | 501   | 0.86×   | 176       |
| 0.21M     | 4000  | 0.69×   | 157       |
| 0.67M     | 501   | 0.75×   | 153       |
| 2.4M      | 500   | 0.74×   | 156       |

setting, geometry is optimized through many gradient-based iterations, where each iteration requires solving a linear system with the same matrix but different right-hand sides. Concretely, the method uses a Laplacian-based operator (fixed per remesh level) to diffuse gradients, leading to repeated solves with a shared factorization. The application also performs periodic remeshing, after which the system is rebuilt and refactorized. As a result, each remesh level exhibits behavior similar to mesh smoothing (§6.4), but with a much larger number of solves per factorization.

Table 2 shows the end-to-end speedup, the application iteration count, and the break-even iteration beyond which the default METIS ordering becomes faster. Unlike mesh smoothing (§6.4), where the per-iteration factorization cost is high and reducing permutation overhead yields an end-to-end speedup, the inverse-rendering workload runs hundreds to thousands of iterations per remesh level while the break-even lies around 100–180 iterations. All five levels run well past break-even, so the slight factor-quality penalty of our patch-based ordering outweighs its permutation savings, and the default METIS ordering is the better choice for this application.

## References

- George Karypis et al. 2013. METIS – Serial Graph Partitioning and Fill-reducing Matrix Ordering. <http://glaros.dtc.umn.edu/gkhome/metis/metis/overview>.
- George Karypis and Vipin Kumar. 1998. A Fast and High Quality Multilevel Scheme for Partitioning Irregular Graphs. *SIAM Journal on Scientific Computing* 20, 1 (1998), 359–392. doi:10.1137/S1064827595287997
- Baptiste Nicolet, Alec Jacobson, and Wenzel Jakob. 2021. Large steps in inverse rendering of geometry. *ACM Trans. Graph.* 40, 6, Article 248 (Dec. 2021), 13 pages. doi:10.1145/3478513.3480501